Available online at www.sciencedirect.com
SCIENCE DIRECT®

Journal of the European Ceramic Society 24 (2004) 2169–2179
www.elsevier.com/locate/jeurceramsoc

Preparation and characterisation of aluminium nitride–titanium nitride composites

Inger-Lise Tangen[a], Yingda Yu[b], Tor Grande[a], Ragnvald Høier[b], Mari-Ann Einarsrud[a,*]

[a]*Department of Materials Technology, Norwegian University of Science and Technology, 7491 Trondheim, Norway*
[b]*Department of Physics, Norwegian University of Science and Technology, 7491 Trondheim, Norway*

Received 24 September 2002; received in revised form 23 April 2003; accepted 2 May 2003

Abstract

Aluminium nitride–titanium nitride (AlN–TiN) composites were prepared to increase the fracture toughness of AlN-based materials. Two methods were used to achieve particle-reinforced materials; TiN (0.3–3.4 vol.%) was formed in-situ or TiN particles (0–21 vol.%) were added. The resulting composites were dense and homogeneous, even at high TiN content. The Vickers hardness and Young's modulus increased when adding 21 vol.% TiN, about 8 and 5%, respectively. SENB measurements showed a 33% increase in fracture toughness when 21 vol.% TiN was added. The toughening mechanism was mainly crack deflection around TiN grains. The fracture toughness was also calculated using various models based on Vickers indentation. The different models underestimated the K_{IC} values compared to the SENB method. The electrical resistivity for materials with low TiN content was high, 10^{8}–10^{14} Ω cm. In the 21 vol.% TiN material the percolation limit of TiN was reached and the resistivity dropped to 10^{-1}–10^{-2} Ω cm.

Keywords: AlN; Composites; Electrical properties; Microstructure-final; Toughness and toughening; TiN

1. Introduction

Aluminium nitride (AlN) ceramics have a unique combination of properties; high thermal conductivity, high corrosion resistance, low dielectric constant, high electrical resistance and low density. AlN is therefore attractive for refractory applications like in metal handling, as heat sinks, in semiconductor devices and electronic substrates, and as grinding media, seals, filler materials, etc. AlN is however a brittle material and for structural applications an increase in mechanical performance i.e. fracture toughness is necessary. Witek et al.[1] reported that fully dense hot-pressed AlN with no sintering additives have a fracture toughness of 3.6±0.3 MPa $m^{1/2}$ (biaxial testing of disk[2]). Huang and Jih[3] reported 3.5–4 MPa $m^{1/2}$ for hot-pressed AlN without sintering additives and Hagen et al.[4] reported 3.6±0.2 MPa $m^{1/2}$ for AlN pressureless sintered with CaO–Al_2O_3 additive, both measured by the single edge notched beam method (SENB). Lower values down to 2.0 MPa $m^{1/2}$ have also been reported.[5–9]

The strategies applied to increase the fracture toughness of AlN-ceramics have been either to optimise the sintering additives or to prepare particle reinforced materials. Terao et al.[10] and Tatami et al.[6] studied mechanical properties of pressureless sintered AlN with Al_2O_3 and Sm_2O_3, La_2O_3 or Y_2O_3 as sintering aids. The La_2O_3 and Sm_2O_3-added samples showed slightly increased mechanical performance compared to Y_2O_3-added samples, i.e. fracture toughness of 3.0–3.1 MPa $m^{1/2}$ (surface crack in flexure method) and bending strength of 407–455 MPa. Witek et al.[1] compared fully dense hot-pressed AlN with no sintering additives and AlN with CaO, and found a decreased hardness, strength and fracture toughness when CaO was added. The fracture toughness decreased from 3.6 to 2.9–3.1 MPa $m^{1/2}$ (biaxial testing of disk[2]). Addition of sintering aids seems to decrease the fracture toughness for AlN compared to pure materials. AlN particle reinforced materials have been made with varying

* Corresponding author. Tel.: +47-73-59-4002; fax: +47-73-59-0860.
E-mail address: mari-ann.einarsrud@material.ntnu.no (M.-A. Einarsrud).

0955-2219/03/$ - see front matter © 2003 Published by Elsevier Ltd.
doi:10.1016/S0955-2219(03)00367-4

non-metallic secondary particles, e.g. TiN,[7,11–13] BN,[8,14] both TiN and BN,[8] and SiC.[3,9,15–20]

TiN is for several reasons an interesting candidate to form composites with AlN. TiN has a higher thermal expansion coefficient ($9{\cdot}10^{-6}$ °C^{-1})[21] than AlN ($4–6{\cdot}10^{-6}$ °C^{-1}),[21] introducing thermal strain in the composites during cooling. Composites can also be designed to have a wide range of electrical resistivity by controlling the microstructure and AlN/TiN-ratio, due to the large difference in electrical resistivities of the pure materials (TiN: $2.3{\cdot}10^{-5}$ Ω cm,[22] AlN: $2{\cdot}10^{11}-10^{14}$ Ω cm,[21,23]). Tajika et al.[7] made pressureless sintered AlN–TiN composites (0–10 vol.% TiN) from the respective powders with yttria as sintering additive and studied the effect of different heat treatments. The fracture toughness increased from 2.8–3.5 to 3.7–4.5 MPa $m^{1/2}$ when 10 vol.% TiN was added and the variation was due to various heat treatments. Tkachenko et al.[11] and Kuzenkova et al.[12] made AlN–TiN composites by hot-pressing and pressureless sintering, respectively. Due to sintering at high temperatures plate-like or filament-like AlN polytypoid grains were formed, which highly influenced the mechanical and electrical properties. AlN–TiN composites have also been made in-situ by Nakahata et al.[13] by adding 0.5 wt.% TiO_2 to an AlN powder mixture. Lattice strain was observed around the TiN-grains and titanium was identified in the AlN matrix. The electric properties of AlN–TiN composites without AlN polytypoids have not been studied, neither have the mechanical properties of high TiN containing composites.

The main goal of this work was to increase the fracture toughness of AlN based materials by preparing AlN–TiN composites using two different synthesis routes. First, TiN particles were synthesised in-situ in the AlN matrix by taking advantage of the chemical reaction between titanium (III) oxide (Ti_2O_3) and AlN according to Eq. (1).

$$Ti_2O_3 + 2\ AlN = 2\ TiN + Al_2O_3 \quad (1)$$

Further, to increase the TiN content without increasing the Al_2O_3 content, composites were made by addition of TiN powder to the AlN powder followed by liquid phase sintering with Al_2O_3–Y_2O_3 as sintering aid. The mechanical and electrical properties of the composites and their dependence on the microstructure were characterized. A comparison of fracture toughness values obtained using the single edge notched beam (SENB) method and various models based on the Vickers indentation method are included.

2. Experimental

In-situ formed AlN–TiN composites were prepared from AlN powder (Tokuyama Soda, Grade F, containing 0.6 wt.% oxygen on the grain surface) and Ti_2O_3 (Alfa Aeser, 99 + % purity). The as received Ti_2O_3 powder was milled to a particle size in the range from 0.1 to 2 μm before use. Y_2O_3 [H.C. Starck, quality Finest, (0.9–3.4 wt.%)] was added to form sintering aid together with alumina formed by reaction [1]. The TiN content of the in-situ composites varied between 0.3 and 3.4 vol.%.

Secondly, to increase the TiN content of the composites without increasing the sintering aid content, composites were prepared from AlN powder (Tokuyama Soda, Grade F) and TiN powder (Alfa Aeser, 99.5% purity). TiN powder in the range from 1 to 2 μm was prepared by sedimentation. Al_2O_3 [Alcoa, A 16 SG (1.7 wt.%)] and Y_2O_3 [H. C. Starck, quality Finest, (0.9 wt.%)] were added as sintering aid. The TiN content in the composites varied between 0 and 21 vol.%.

The powders were mixed in 100% ethanol by ball milling for 4 h using alumina balls. Soft agglomerates (< 500 μm) were formed by sieving before preparation of bars for mechanical testing. The powder was either uniaxially pressed into pellets (15 $mm^{\varnothing}$) at 230 MPa or into bars, which were first uniaxially pressed at 15 MPa and then isostatically pressed at 200 MPa. Ethyl cellulose (Sigma) (2 wt.%) was used as binder. The green density of both bars and pellets was approximately 56%.

The samples were sintered in N_2-atmosphere in a graphite resistance furnace.[24] The pellets were sintered in a molybdenum (Mo) crucible with a Mo lid and the bars were sintered in a graphite-crucible lined with Mo-foil. The heating rate was 2000 K/h from 600 °C up to 1650 °C and 1000 K/h up to the sintering temperature of 1870 °C where the samples were kept for 6 h. The cooling rate was 1000 K/h from the sintering temperature to 1650 °C and 2000 K/h to approximately 400 °C. The density was determined by Archimedes' method using isopropanol and the theoretical density was calculated from the law of mixtures. The theoretical density was not corrected for weight loss during sintering.

The microstructure of the samples was studied by scanning electron microscopy (SEM) (Zeiss DSM 940), transmission electron microscopy (TEM) (Philips CM30) equipped with energy dispersive spectroscope (EDS) (Edax International) and high resolution TEM (HRTEM) (JEM-2000F). TEM specimens were prepared by cutting 0.5 mm thick slices from the interior of the samples and 3 mm diameter discs were cut from these. The discs were mechanically ground to approximate thickness of 150 μm, and further thinned using a dimple grinder, until the central region of the specimens were about 30 μm thick. Final electron transparency was obtained by ion beam thinning. Phase composition was studied by powder X-ray diffraction (XRD) using a Siemens D5005 X-ray diffractometer. The samples were ground to powder prior to XRD measurements. Silicon

powder (10–15 wt.%) was added as an internal standard for *d*-value calibration. Lattice parameters were calculated using the programs Win-Index and Win-Metric from Bruker axs. The grain size of the sintered samples was measured on polished surfaces thermally etched at 1600 °C for 0.2 h. About 200–700 AlN grains were measured using the linear intercept method and 500–900 TiN grains were measured directly.

Bending strength and Young's modulus (E-modulus) were measured using a four point bending test. Sample bars were machined to MIL SPEC 1942 and dimensions $4\times3\times45$ mm^3. All the edges were chamfered. The testing was performed in a 4-point flexure 40/20 mm span in a Dartec 20 kN Servohydraulic Universal Testing machine with a 20 kN load cell. Displacement was measured by a displacement gauge of the Tesa type, placed in contact with the specimen in the centre of the span. The displacement gauge was fixed and measured the displacement relative to the support rollers. Loading point and supports were free to roll, diameter of these were 4.9 mm. All measurements were performed in displacement control at a crosshead rate of 0.5 mm/min. A total of 6–9 specimens were tested for each composition. The fracture surfaces were studied by SEM to reveal the fracture origins.

The fracture toughness was determined using the single edge notched beam method (SENB). The room temperature testing was performed in an Instron 1126 Universal Electromechanical Machine using a 250 N load cell. The fracture toughness at 800 °C in flowing N_2 atmosphere (max 230 ppm O_2) was measured using a Cormet 20 kN Electromechanical machine with a 2 kN HBM load cell and a Sigmatest furnace with Kanthal A element and nickel radiation shields. A four-point SiC bending fixture (MTS, 642.85) was used. The sample bar dimensions for all measurements were $4\times3\times45$ mm^3, all machined to MIL SPEC 1942. The depth of the notches was 1.2 mm and the width about 0.2 mm. Fracture toughness was calculated using ISO 15732.[25] A total of 3–4 specimens were tested for each composition.

Hardness was measured using the Vickers indentation method on polished surfaces. Fracture toughness was also determined from indents at high load to compare to the values obtained by the SENB method. An Akashi AVK-C1 Hardness Tester was used for the indentation and a Reickert MeF3 A optical microscope with a Sony DXC-930P Colour Video Camera and the program NIH Image were used for measuring of indents and crack lengths. Vickers hardness, H_V, was calculated using the equation reported by Anstis et al.[26] and fracture toughness was calculated from various different equations presented by Ponton and Rawlings.[27] Vickers hardness was calculated from 2.9 N indents and fracture toughness from 49.05 N indents. Ten indents were measured for each composition and load.

The electrical resistivity was measured by a four-point method using silverbased electrodes and a Quadtech 1865 Megohmeter (AlN and 10 vol.% TiN) or a Fluke Handheld Digital Multimeter (21 vol.% TiN). Measurements were performed in air (AlN) or in flowing nitrogen (10 and 21 vol.% TiN) up to 550 °C. The sample dimensions were $4\times3\times22$ mm^3. Three samples were measured for each composition.

3. Results

All the samples obtained high relative density (>98% of theoretical) after sintering regardless of TiN content, which shows that the sintering conditions used are efficient. Yttrium aluminium perovskite (YAP), $AlYO_3$, were identified by XRD as the secondary phase in all the pellets and yttria aluminium garnet (YAG), $Al_5Y_3O_{12}$ in the bars for mechanical testing. The secondary phases identified are dependent on the crystallisation path of the AlN containing Al_2O_3–Y_2O_3 liquid formed during sintering. According to the quasi-binary Y_2O_3–Al_2O_3 phase diagram[28] the samples were expected to contain alumina and YAG or, assuming a metastable situation, alumina and YAP. YAP is stabilised in the quasi-quaternary AlN–YN–Al_2O_3–Y_2O_3 system compared to the quasi-binary system, but the solid solubility of nitrogen in both YAG and YAP is low.[29] The apparent lack of alumina or AlON-spinel in all the samples after sintering and an observed weight loss of 1–2% can be explained by evaporation of $Al_2O(g)$ according to Eq. (2).[4]

$$Al_2O_3 + 4\ AlN = 3\ Al_2O(g) + 2\ N_2(g) \quad (2)$$

XRD investigations of a layer formed on the inside of the lid of the Mo crucible used during sintering identified AlN. This supports the theory of evaporation of $Al_2O(g)$ which forms AlN on reaction with N_2. The

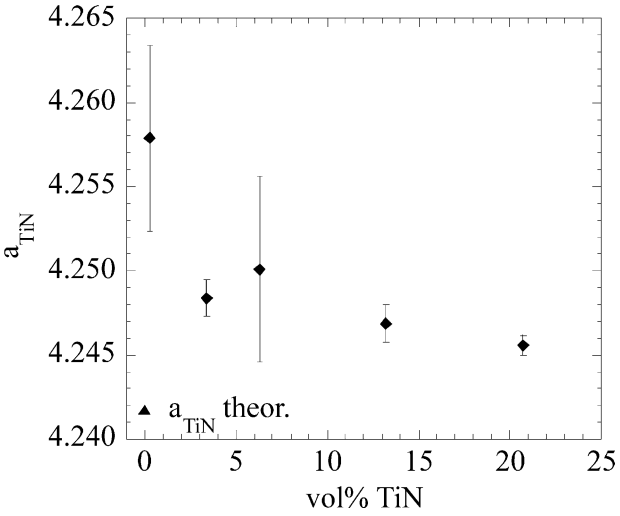

Fig. 1. Lattice parameter of TiN in AlN–TiN composites vs. TiN content. The theoretical value of a_{TiN} is also included.[30]

evaporation shifted the assumed composition of the liquid phase 4–8 mol% towards Y_2O_3. The weight loss showed no systematic changes with TiN content or between pellets and bars.

The XRD investigations also showed that the lattice parameter for TiN decreases towards the theoretical value (4.24173 Å)[30] with increasing TiN content of the composites (Fig. 1). According to Inamura et al.,[31] the TiN lattice parameter decreases linearly with increasing aluminium content, and aluminium is hence not responsible for the increased values observed. Both TiO and YN have the same cubic structure as TiN with lattice parameters of 4.1850 Å[32] and 4.89440 Å,[33] respectively. Hence only a solid solution of YN in the TiN can explain the increased lattice parameter. Nakahata et al.[13] also reported high lattice parameters for TiN, 4.261 Å, for a AlN–TiN composite with yttria as sintering additive.

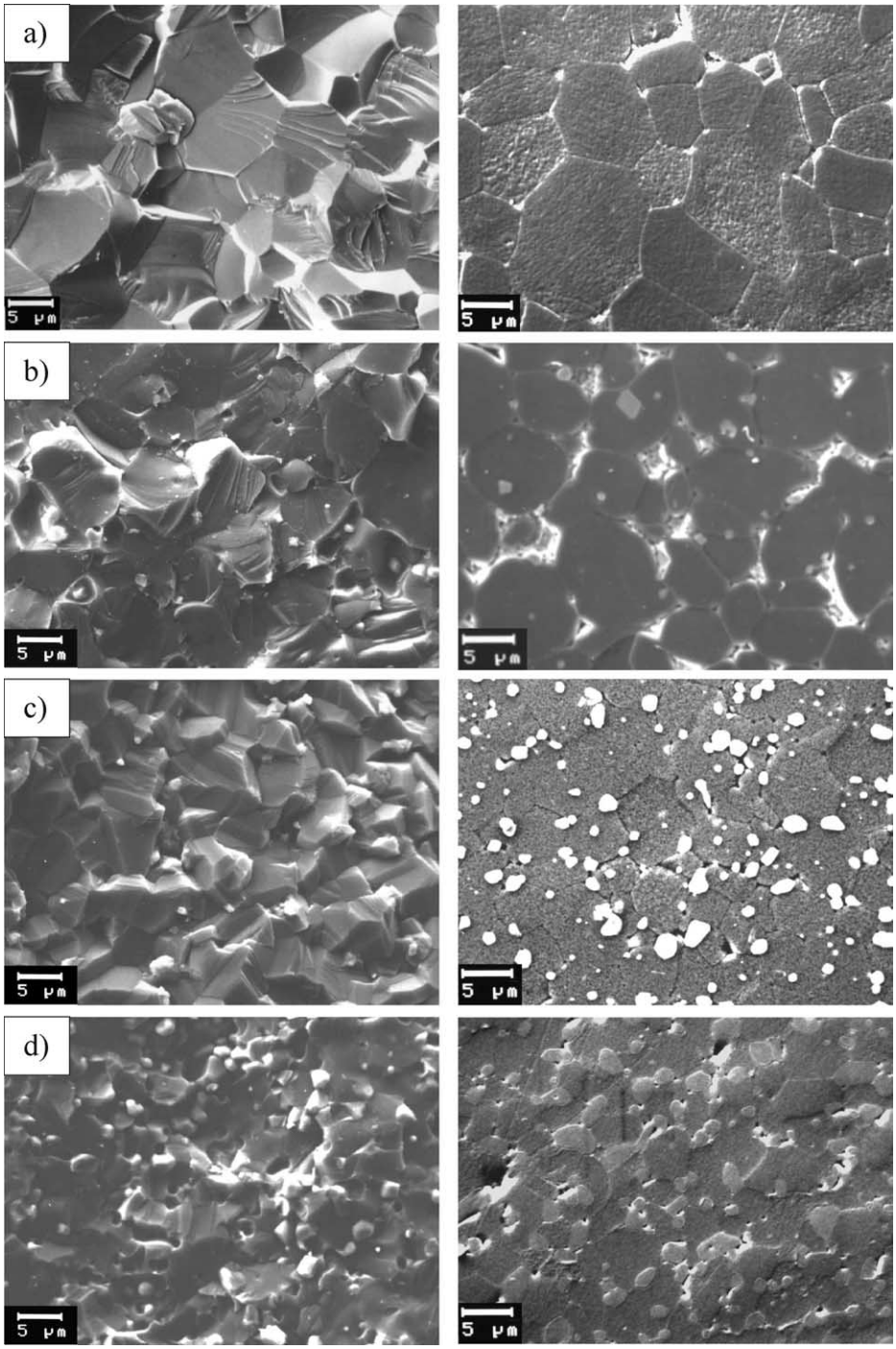

Fig. 2. SEM images of fracture surfaces and polished and etched surfaces of AlN and AlN–TiN composites. The lighter grains are TiN. (a) AlN, (b) 3.4 vol.% in-situ formed TiN (8 wt.% sintering additive), (c) 10 vol.% added TiN and (d) 21 vol.% added TiN.

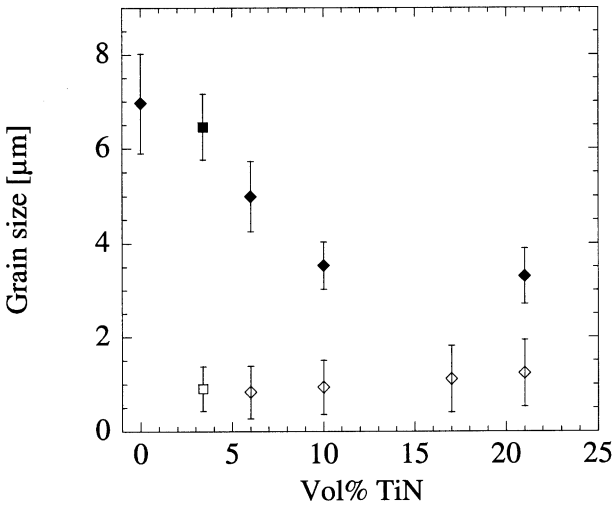

Fig. 3. Grain size of AlN (filled symbols) and TiN grains (open symbols) in AlN and AlN–TiN composites. The diamonds represent added TiN-composites and the squares represent in-situ composites. The error bars represent the variation in grain size.

SEM images of fracture surfaces of AlN and AlN–TiN composites containing 3.4–21 vol.% TiN are shown in Fig. 2 together with corresponding SEM images from polished and thermally etched surfaces. Both the fracture surfaces and the polished surfaces show a homogeneous distribution of inter- and intragranular TiN-grains. The fracture surfaces show mainly transgranular fractures of the AlN-grains. The size of the AlN grains decreases with increasing amounts of TiN as can be seen in Fig. 3, where the measured grain sizes for both TiN and AlN are plotted. The size of the AlN grains decreases with TiN-addition up to 10 vol.%. These results show that the larger TiN grains act as grain boundary pinning centres during sintering. The smaller TiN grains can not slow down the movement of AlN grain boundaries and are therefore incorporated into the AlN grains. Similar AlN grain growth inhibitation and the distribution of large and small TiN grains were observed by Tajika et al.[34] in AlN–TiN composites with up to 10 wt.% TiN. The TiN grain size increases

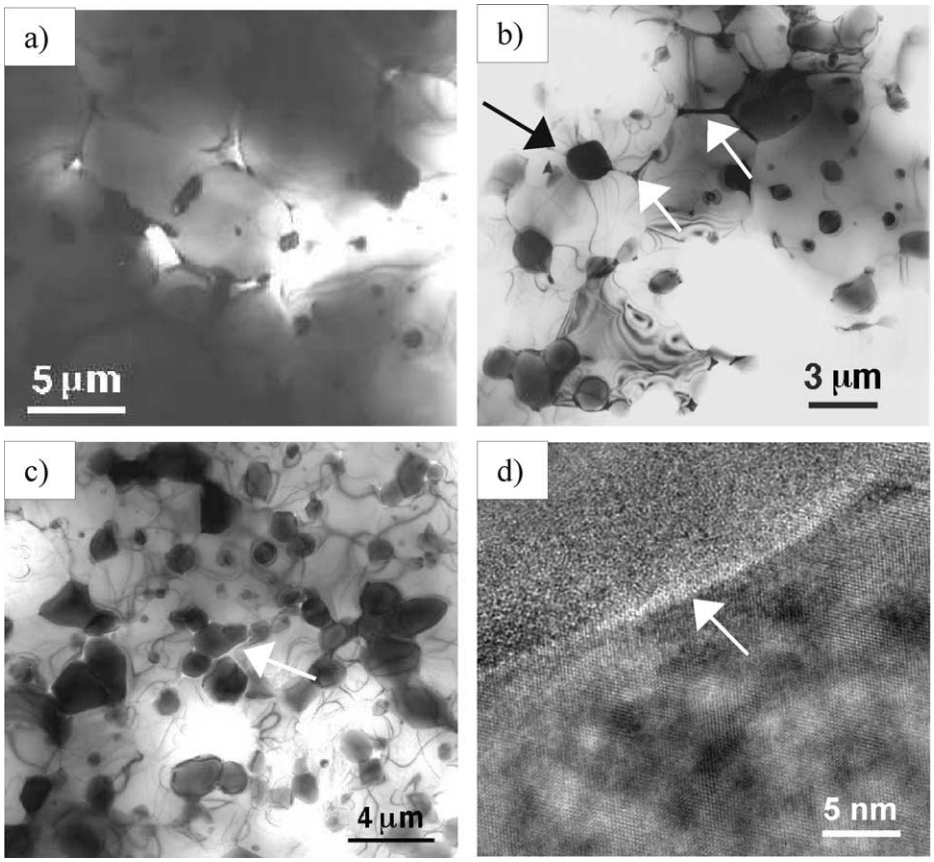

Fig. 4. Low magnification TEM images and HRTEM image of AlN-TiN composites. The dark contrast grains are TiN. (a) 3.4 vol.% in-situ formed TiN (8 wt.% sintering additive), (b) 10 vol.% added TiN (black arrow shows residual strain around a TiN grain, the white arrows show sintering additive phases at grain boundaries and triple junctions), (c) 21 vol.% added TiN (white arrow shows open pores associated with large intergranular TiN grains) and (d) HRTEM image showing a grain boundary between an intragranular TiN grain (lower grain) and AlN (upper) in the sample containing 10 vol.% added TiN. The arrow shows the amorphous grain boundary.

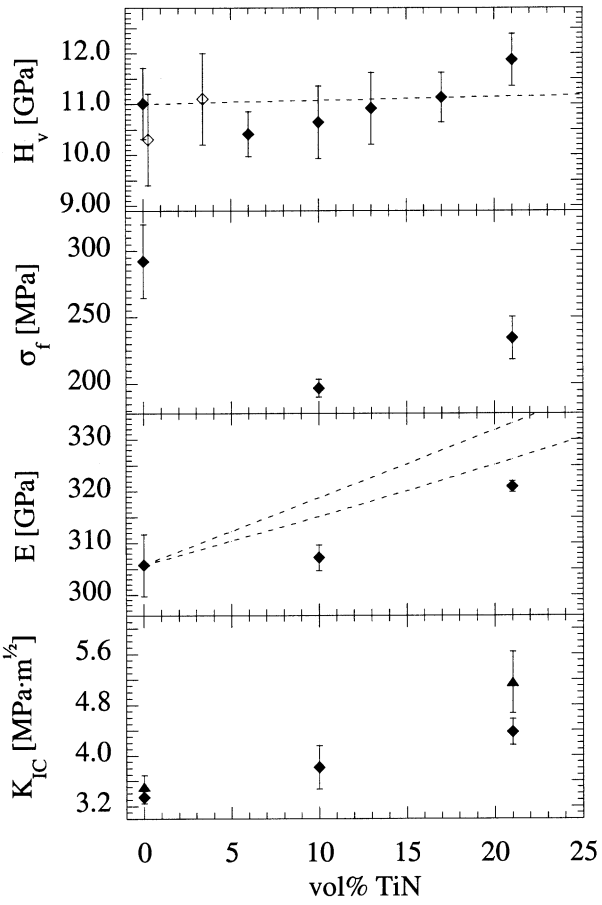

Fig. 5. Vickers hardness, 4-point bending strength, E-modulus and fracture toughness (SENB method) of AlN and AlN–TiN composites versus TiN content. Closed symbols represent composites with added TiN while open symbols represent in-situ formed composites. The triangles are measurements performed at 800 °C. The dotted line in the hardness plot is the linear mixing between Vickers hardness for pure TiN and AlN. The dotted lines in the E-modulus plot are the upper (Voigt model) and lower (Reuss model) bounds of the Young's modulus in composite materials.[22,37] The error bars represents standard deviations.

slightly with increasing TiN content, probably caused by liquid phase sintering.

Low magnification TEM images of the samples containing 3.4 vol.% in-situ formed TiN and 10 and 21 vol.% added TiN are presented in Fig. 4. The light contrast grains are AlN and both TiN and secondary phases (YAG and YAP) are seen as dark contrast. The secondary phases are mainly located at triple junctions and along some of the grain boundaries (white arrows in Fig. 4b).

The TEM images clearly confirm that the smaller TiN grains (diameter below 1 μm) are predominately observed intragranulary whereas larger grains (normally below 3 μm) are situated intergranulary. The TiN grains give rise to local residual strain contrasts in the surrounding AlN matrix, as shown by the black arrow in Fig. 4b. The strain is probably generated due to thermal expansion mismatch between the two different materials. Nakahata et al.[13] also observed strain in the AlN matrix surrounding TiN grains, but they ascribed this to Ti-ions dissolved in the AlN lattice. XRD-investigations showed no significant change in the lattice parameter of the AlN matrix relative to pure AlN, but a small amount of titanium was identified in the AlN-matrix by TEM/EDS. The large intergranular TiN grains were observed to be associated with open pores and Fig. 4c shows typical pore regions. These pores might be formed during cooling from the sintering temperature if the AlN grains are better wetted by the liquid phase than the TiN grains. Between the small intragranular grains and the hosting AlN grains an amorphous layer was observed as can be seen from the HRTEM image in Fig. 4d. This amorphous layer is probably related to the intergranular secondary phase.

Vickers hardness, bending strength, Young's modulus and fracture toughness are plotted as a function of vol.% TiN in Fig. 5. The hardness is increasing by approximately 8% when adding 21 vol.% TiN. The law

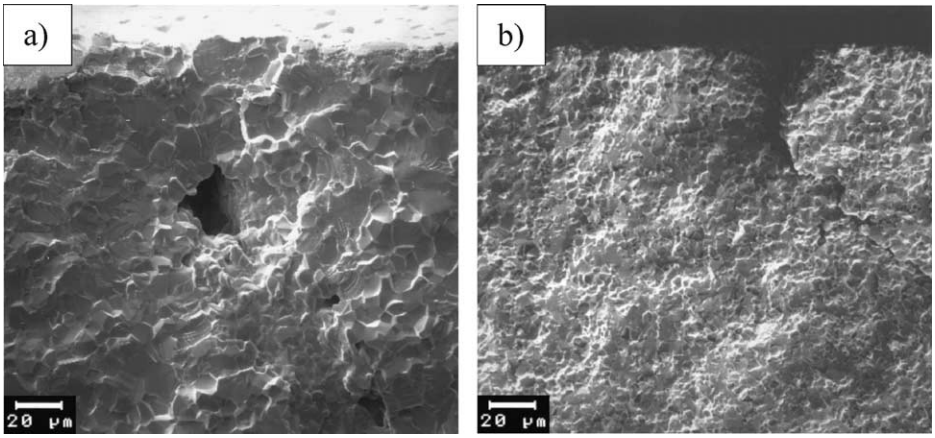

Fig. 6. Fracture origins of samples used for bending strength measurements. (a) Open pore inside bar (AlN) and (b) Surface pore extended into the bar (10 vol.% TiN).

of mixtures between the two pure materials (TiN: 11.7±0.4 GPa)[22] is included in Fig. 5 and the measured values show the same trend. There are no significant differences between the in-situ made samples and the samples with added TiN. Tajika et al.[7] observed an increase in Vickers hardness, from 9.8 to 10.3 GPa when adding 10 vol.% TiN to AlN.

The bending strength of pure AlN was determined to be 281±39 MPa, which is in agreement with literature values.[3,4,6,35] The bending strength shows a minimum for 10 vol.% TiN. The fracture origins from the bending strength measurements were pores as can be seen from selected fractographs given in Fig. 6. These pores can either be formed from volatile contaminations in the powder or inhomogeneous packing of the green body. A few areas of high TiN-grain concentration were detected on the fracture surfaces. However, these areas were far from the fracture origins, but an influence on the bending strength can not be excluded. Generally the fracture strength is expected to increase with decreasing grain size,[36] opposite of the observed trend (Fig. 3). The bending strength therefore seems to be more determined by inhomogeneities in the samples than by the material properties. The fracture surfaces given in Fig. 6 have a larger part of intergranular fractures compared to the fracture surfaces presented in Fig. 2, probably caused by different crack growth during fracture testing and formation of fracture surfaces.

The E-modulus is presented in Fig. 5 together with the Voigt model (upper bounds) and the Reuss model (lower bounds) for E modulus of a AlN–TiN composite.[22,37] Adding 21 vol.% TiN gave a 5% increase and the observed values for the AlN–TiN-composites are closer to the lower bound (Reuss) model. The E-modulus for pure AlN was found to be 306±6 GPa which is in accordance with data reported in the literature.[1,4,5,35]

The fracture toughness value for pure AlN measured by the SENB method was 3.3±0.1 MPa $m^{1/2}$ (Fig. 5) which is slightly lower than the values reported in the literature.[1,3,4] The fracture toughness increases 33% when adding 21 vol.% TiN, giving the value of 4.4±0.2 MPa $m^{1/2}$. This value is significantly higher than values reported for pure AlN[1,3,4] and comparable to other ceramic materials like SiC (3.0–3.5 MPa $m^{1/2}$), Si_3N_4 (4–6 MPa $m^{1/2}$) and Al_2O_3 (3.5–4.0 MPa $m^{1/2}$) (not in-situ composites/self-reinforced materials).[38] For AlN with 10 vol.% TiN, Tajika et al.[7] reported 3.7–4.5 MPa $m^{1/2}$, which is comparable to the value 3.8±0.3 MPa $m^{1/2}$ obtained in this study. Tajika et al.[8] also report increased fracture toughness, from 2.9 to 4.2 MPa $m^{1/2}$, when adding 5 vol.% TiN to AlN–10% BN composites.

The fracture toughness at 800 °C was somewhat higher than at room temperature. AlN exhibited a 5% increase in fracture toughness while the composite containing 21 vol.% TiN showed a 18% increase to 5.1±0.5 MPa $m^{1/2}$ at 800 °C. AlN also showed a change from mainly intergranular fractures at room temperature to mainly transgranular fractures at 800 °C.

The room temperature fracture toughness was also determined from Vickers indents at high load (49.05 N).

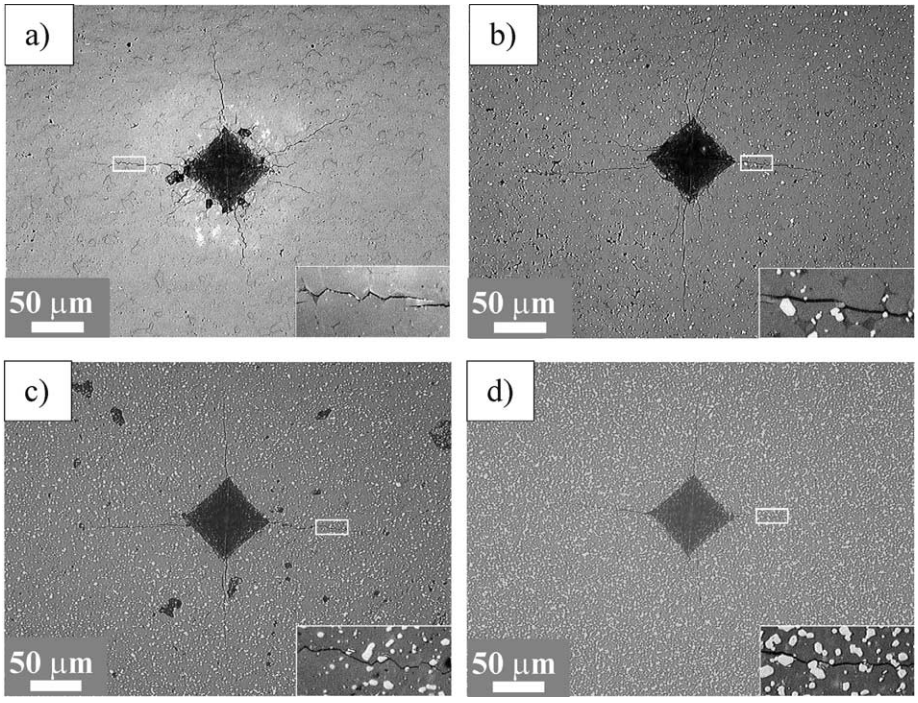

Fig. 7. Optical microscope images showing Vickers indents (49.05 N) in AlN and AlN-TiN composites. The light contrast grains are TiN. (a) AlN, (b) 3.4 vol.% in-situ formed TiN (8 wt.% sintering additive), (c) 10 vol.% added TiN and (d) 21 vol.% added TiN. 5× enlargement of crack in the right corner of each image.

Optical microscope images of selected indents are shown in Fig. 7. The cracks propagate mainly transgranulary through the AlN matrix as was also seen in Fig. 2. Also the sample with 8 wt.% sintering additive (3.4 vol.% in situ formed TiN) have this crack behaviour. The cracks are deflected by the TiN-grains as predicted by the difference in thermal expansion coefficient.[21]

Several different models for calculation of the fracture toughness based on cracks from Vickers indents are gathered and rearranged to a standard form by Ponton and Rawlings[27] and Fig. 8 shows the fracture toughness calculated from selected models together with the measured crack length. The values obtained by the SENB method are included for comparison. The different models generally underestimate the fracture toughness and the values vary much from one model to another. None of the models gives a clear increase with increasing TiN content. Most the models show a relatively high value for the pure AlN sample because of the short measured crack length for this sample. The short apparent crack length might be due to formation of several cracks from the indent (Fig. 7a) and will overestimate the fracture toughness.

The electrical resistivity as a function of temperature for three selected materials is given in Fig. 9. The samples with $\leqslant$10 vol.% TiN have a high resistivity which decreases with increasing temperature, and the sample with 10 vol.% TiN has a resistivity two to three decades higher than AlN. The resistivity of the composite containing 21 vol.% TiN is low (10^{-1}–10^{-2} Ω cm) and increases slightly with temperature.

4. Discussion

All the prepared materials were dense, homogeneous and had the expected phase composition. The major microstructural difference between the samples was the grain size of AlN, which decreased when adding TiN. The sintering additive phases were similar within the two groups of materials, pellets and bars. The grain size of the AlN grains, the TiN content and any possible inhomogeneities should therefore determine the mechanical properties.

As shown in Fig. 5, the fracture toughness increases with increasing TiN in the ceramics. The main reason for the toughening is crack deflection around TiN grains caused by the different thermal expansion of TiN and AlN. The residual strain is clearly observed from the TEM-investigations. Tajika et al.[7] refers to a micromechanic approach to explain the improved mechanical properties for AlN–TiN composites, but do not describe a mechanism.

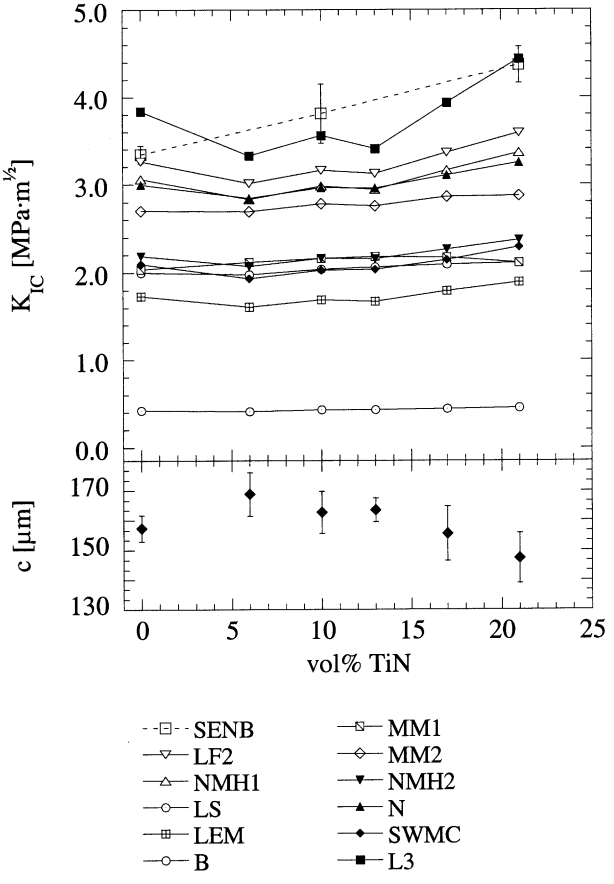

Fig. 8. Fracture toughness calculated from crack lengths of Vickers indents versus TiN content. SENB results are included. The lower part shows the average crack length. The open symbols represent models based on radial-median crack geometry and the filled symbols models based on Palmqvist crack geometry. All the calculations are based on the models as they are presented by Ponton and Rawlings. Also the abbreviations of the different models are obtained from Ponton and Rawlings.[27]

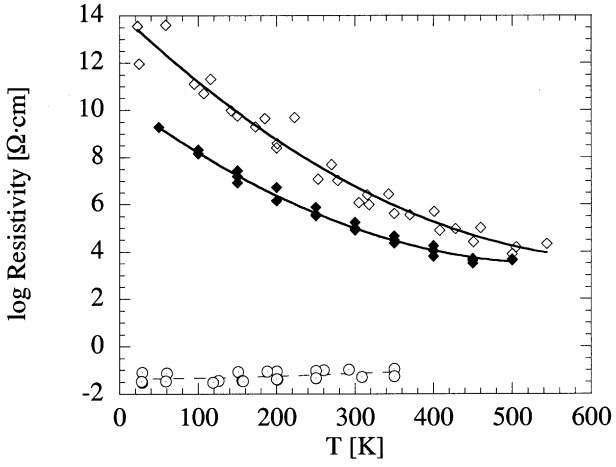

Fig. 9. Electrical resistivity versus temperature for AlN and AlN–TiN composites. The filled diamonds represent pure AlN, the open diamonds 10 vol.% added TiN and the open circles represent 21 vol.% added TiN composites. Equations of the line fittings: Pure AlN: log $R = 2.2\cdot10^{-5}\cdot T^2 - 0.025\cdot T + 10.5$; 10 vol.% TiN log $R = 2.4\cdot10^{-5}\cdot T^2 - 0.032\cdot T + 14.1$; 21 vol.% TiN log $R = 1.7\cdot10^{-6}\cdot T^2 - 0.00027\cdot T + 1.4$.

The increase in fracture toughness is not highly influenced by the grain size of AlN as the increase in toughness is linear from 0 to 21 vol.% TiN while the grain size of AlN decreases when adding up to 10 vol.% TiN, from where it is rather constant (Fig. 3). The non-dependence of K_{IC} on the AlN grain size can be explained by the transgranular fracture mode. For a material with transgranular fracture mode, the crack path will not be lengthened by increasing grain size and the fracture toughness will not be influenced. A small increase in K_{IC} might be seen if the crack path changes direction from one grain to another, i.e. to follow specific atomic planes. This behaviour is observed in the AlN-materials, especially in Fig. 2c. The transgranular mode of fracture indicates a strong grain boundary phase.

No deterioration of the fracture toughness was observed at 800 °C confirming no secondary phase creep at this temperature (melting at 1816 °C[28]). Actually, an increase in fracture toughness was observed which might be due to the fact that the high temperature measurements were performed in nitrogen and the room temperature measurements in air. Hence, at room temperature humidity might give corrosion during fracture growth. The fracture mode in the pure AlN material changes from mainly intergranular at room temperature to mainly transgranular at 800 °C without a corresponding drop in fracture toughness. These results substantiate that crack deflection due to preferred crack growth direction in single grains toughens the pure AlN material.

The models used in Fig. 8 to estimate room temperature fracture toughness from indents underestimate the fracture toughness. For some of the models the values are only ~1/10 of the values measured by the SENB method. Some underestimation is expected due to the higher flaw size in SENB measurements compared to the indentation techniques and expected R-curve behaviour.[39] The model giving the best fit to the values measured by the SENB method, is the model given by Laugier[40] based on a Palmqvist crack geometry. In this model the individual Palmqvist cracks are represented as semicircles. Generally the models based on the Palmqvist geometry give higher K_{IC} values than most the models based on penny-like geometry and therefore give values closer to the ones obtained by the SENB-method. Most models presented in Fig. 8 show increasing fracture toughness as the TiN content is increased, but a smaller increase than the SENB-method. The resulting conclusion of this comparative study is that it is difficult to obtain reliable fracture toughness values using the indentation method, at least for this type of ceramic materials. The indentation method is mostly predicting the same trend in the fracture toughness as the SENB method, however some deviations are present (Fig. 8). It is therefore important to report the method used for fracture toughness determination and the calculating model used if an indentation method is chosen. These results also infer that the fracture toughness measured by SENB in this study and by indentation techniques by Tajika et al.[7] are not directly comparable.

The electrical resistivity of AlN–TiN composites can be described by percolation theory, effective media theories (Bruggeman's theory)[41] and general effective media (GEM) theories,[42] based on the electrical resistivity of the phases, the volume fraction of the different phases, and geometrical/connectivity parameters. The critical volume fraction, or percolation limit, is the volume fraction of the conducting phase when a continuous framework of the conductive phase is formed. The 21 vol.% TiN material is close to the percolation limit of the AlN–TiN system and shows a large decrease in resistivity compared to the pure AlN and 10 vol.% TiN material when low resistivity TiN ($2.30 \cdot 10^{-5}$ Ω cm)[22] form a continuous framework in the high resistivity AlN matrix ($2 \cdot 10^{11}$–10^{14} Ω cm).[21,23] The percolation limit typically varies between 0.01 and 0.6 and the "basic" value is about 0.16 when the grains of conductive and non-conductive phase are near spherical and near equal in size.[42] The pure AlN samples have low resistivity at room temperature compared to literature value however the resistivity is increased by addition of 10 vol.% TiN. The largest differences between these two materials are the TiN content and the grain size. There are no reasons why addition of TiN should increase the resistivity as TiN has a lower resistivity than AlN. Due to the smaller grain size in the 10 vol.% TiN material the continuity of the secondary phase, YAG, is expected to be lower compared to the pure AlN material. YAG has an even higher resistivity than AlN, electrical conductivity of 10^{-16} S/m at 386 °C,[43] i.e. resistivity higher than 10^{14} Ω cm at room temperature, and the YAG distribution can therefore not explain the unexpected low resistivity of the AlN material. The resistivity measurements show that it is possible to design the electrical resistivity of AlN–TiN composites by modifying the AlN/TiN-ratio and the microstructure.

5. Conclusions

Dense and homogeneous AlN–TiN composites were prepared by pressureless sintering. The larger TiN grains acted as grain boundary pinning centres during sintering and were found intergranular, while the smaller TiN grains were found intragranular. The Vickers hardness and Young's modulus increased slightly when adding 21 vol.% TiN, about 8 and 5%, respectively, and the bending strength of the composite material showed a minimum for 10 vol.% TiN. The results obtained by the SENB method showed a 33% increase

in fracture toughness when 21 vol.% TiN was added. The toughening mechanism was mainly crack deflection around TiN caused by different thermal expansions of AlN and TiN. The electrical resistivity for materials with low TiN content was high, 10^8–10^{14} Ω cm, and decreasing with temperature. When adding 21 vol.% TiN the percolation limit was reached, hence a continuous TiN-network was formed and the resistivity dropped to 10^{-1}–10^{-2} Ω cm.

Acknowledgements

The Research Council of Norway is acknowledged for financial support. PhD Kristin Breder is acknowledged for help with developing the method for fracture toughness measurements. We are grateful to Watlow Electric Manufacturing Company, Fenton, MO, USA for measurement of the electrical resistivity of selected samples.

References

1. Witek, S. R., Miller, G. A. and Harmer, M. P., Effects of CaO on the strength and toughness of AlN. *J. Am. Ceram. Soc*., 1987, **72**, 469–473.
2. Cook, R. F., Lawn, B. R. and Fairbanks, C. J., Microstructure—strength properties in ceramics: I, Effect of crack size on toughness. *J. Am. Ceram. Soc*., 1985, **68**, 604–615.
3. Huang, J.-L. and Jih, J.-M., Investigation of SiC-AlN: Part II, Mechanical properties. *J. Am. Ceram. Soc*., 1996, **79**, 1262–1264.
4. Hagen, E., Yu, Y. D., Grande, T., Høier, R. and Einarsrud, M.-A., Sintering of AlN ceramics using CaO–Al_2O_3 as sintering additive—chemistry and microstructural development. *J. Am. Ceram. Soc*., 2002, **85**, 2971–2976.
5. Hunold, H., Herstellung, Eigenschaften und Anwendungsmöglichkeiten von Aluminiumnitrid-Bauteilen. *Metall*., 1990, **3**, 266–269.
6. Tatami, J., Komeya, K., Meguro, T., Iwasawa, S. and Terao, R., Fracture behaviour of strengthened AlN. *Ceram. Trans*., 2000, **106**, 494–499.
7. Tajika, M., Matsubara, H. and Rafaniello, W., Microstructures and properties in aluminium nitride-titanium nitride composite ceramics. *Mater. Lett*., 1999, **41**, 139–144.
8. Tajika, M., Matsubara, H., Rafaniello, W. and Hojo, J., Development of synergistic AlN ceramics by simultaneous addition of BN and TiN. *J. Mater. Sci. Lett*., 2001, **20**, 201–203.
9. Li, J.-F. and Watanabe, R., Pressureless sintering and high-temperature strength of SiC-AlN ceramics. *J. Ceram. Soc. Jpn*., 1994, **102**, 727–731.
10. Terao, R., Tatami, J., Meguro, T. and Komeya, K., Fracture behaviour of AlN ceramics with rare earth oxides. *J. Eur. Ceram. Soc*., 2002, **22**, 1051–1059.
11. Tkachenko, Y. G., Yirchenko, D. Z., Oleinik, G. S., Shevchenko, O. A. and Satanin, S. A., Self-reinforced materials based on aluminium nitride. *Sov. Powder Metall*., 1992, **31**, 785–789.
12. Kuzenkova, M. A., Kislyi, P. S. and Pshenichaya, O. V., Structure and properties of composites based on Ti, Zr and Al nitrides. *Izv. Akad. Nauk SSSR, Neorg. Mater*., 1976, **12**, 430–434 (= Inorg. Mater., 1976, 12, 371–374).
13. Nakahata, S., Matsuura, T., Sogabe, K., Yamakawa, A., Analysis of Ti compound particle distribution in AlN-matrix composites, *Ceram. Trans*. 44 (The American Ceramic Society) 221–231.
14. Mazdiyasn, K. S., Ruh, R. and Hermes, E. E., Phase characterization and properties of AlN-BN composites. *Am. Ceram. Soc. Bull*., 1985, **64**, 1149–1154.
15. Huang, J.-L. and Jih, J.-M., Investigation of SiC–AlN: Part I, Microstructure and solid solution. *J. Mater. Res*., 1995, **10**, 651–658.
16. Lee, R.-R. and Wei, W.-C., Fabrication, microstructure and properties of SiC–AlN ceramic alloys. *Ceram. Eng. Sci. Proc*., 1990, **11**, 1094–1121.
17. Kobayashi, Y., Li, J. F., Kawasaki, A. and Watanabe, R., Microstructure and high-temperature property of reaction HIP-sintered SiC–AlN ceramic alloys. *Mater. Trans*., 1996, **37**, 807–812.
18. Melnikova, V. A., Kazakov, V. K. and Pilyankevich, A. N., Structure of ceramics of the AlN-SiC system. *Sov. Powder. Metall*., 1988, **27**, 498–502.
19. Mariano, S. A., Friel, D. and Bar-On, I., Elevated temperature mechanical properties of SiC-AlN particulate composites. *Ceram. Eng. Proc*., 1993, **14**, 1077–1088.
20. Tangen, I.-L., Yu, Y. D., Grande, T., Høier, R., Mokkelbost, T., Einarsrud, M.-A., Preparation and characterisation of aluminium nitride–silicon carbide composites. *Ceram. Int*. (submitted for publication).
21. Shackelford, J. F., Alexander, W. and Park, J. S., *CRC Materials Science and Engineering Handbook*, 2nd edn. CRC Press, Boca Raton, 1994.
22. Graziani, T. and Bellosi, A., Densification and characteristics of TiN ceramics. *J. Mater. Sci. Lett*., 1995, **14**, 1078–1081.
23. Baik, Y. and Drew, R. A. L., Aluminium nitride: Processing and applications. *Key Eng. Mater*., 1996, **122–124**, 553–570.
24. Herstad, O. and Motzfeldt, K., Vapour pressures in the system Al–Al_2O_3. The effusion method and pressure compensation methods. Rev. Hautes Temper. *Et Réfract*., 1966, **3**, 291–300.
25. ISO/CD 15732 Fine ceramics (Advanced ceramics, Advanced technical ceramics)—Test method for fracture toughness at room temperature by single edge precracked beam (SEPB) method. International Organization for Standardization, Geneva, Switzerland.
26. Anstis, G. R., Chantikul, P., Lawn, B. R. and Marshall, D. B., A critical evaluation of indentation techniques for measuring fracture toughness: I, Direct crack measurements. *J. Am. Ceram. Soc*., 1981, **64**, 533–538.
27. Ponton, C. B. and Rawlings, R. D., Vickers indentation fracture toughness test Part 1 Review of literature and formulation of standardised indentation toughness equations. *Mater. Sci. and Techn*., 1989, **5**, 865–872.
28. Gröbner, J., Lukas, H. L. and Aldinger, F., Thermodynamic calculations of the quasibinary Al_2O_3–Y_2O_3 system and the Y–Al–O ternary system. *Z. Metallkd*., 1996, **87**, 268–273.
29. Sun, W. Y., Huang, Z. K., Tien, T. Y. and Yen, T. S., Phase relationships in the system Y–Al–O–N. *Mater. Lett*., 1991, **11**, 67–69.
30. Wong-Ng, W., McMurdie, H. F., Paretzkin, B., Zhang, Y., Davis, K. L., Hubbard, C. R., Dragoo, A. L. and Stewart, J. M., Standard x-ray diffraction powder patterns of sixteen ceramic phases. *Powder Diffr., (PDF 38-1420)*, 1987, **2**, 191–201.
31. Inamura, S., Nobugai, K. and Kanamura, F., The preparation of NaCl-Type $Ti_{1-x}Al_xN$ solid solution. *J. Solid State Chem*., 1987, **68**, 124–127.
32. Loehman, R. E., Rao, C. N. R. and Honig, J. M., Crystallography and defect chemistry of solid solutions of vanadium and titanium oxides. *J. Phys. Chem., (PDF 77-2170)*, 1969, **73**, 1781.
33. Kempter, C. P., Krikorian, N. H. and McGuire, J. C., The crystal structure of yttrium nitride. *J. Phys. Chem., (PDF 35-779)*, 1957, **61**, 1237–1238.

34. Tajika, M., Nomura, H., Matsubara, H. and Rafaniello, W., Experimental and computational study of grain growth and microstructures in AlN composites ceramics. *J. Ceram. Soc. Jpn*., 2001, **109**, 288–293.
35. Marchant, D. D. and Nemecek, T. E., Aluminium nitride: Preparations, processing and properties. In *Advances in Ceramics: Ceramic Substrates and Packages for Electronic Applications*, ed. M. F. Yan, K. Niwa, H. M. O'Bryan and W. S. Young. Am Ceram Soc, Westerville, Ohio, 1989, pp. 19–54.
36. Knudsen, F. P., Dependence of mechanical strength of brittle polycrystalline specimens on porosity and grain size. *J. Am. Ceram. Soc*., 1959, **42**, 376–387.
37. Kingery, W. D., Bowen, H. K. and Uhlmann, D. R., *Introduction to ceramics*. John Wiley & Sons, New York, 1976.
38. Richerson, D. W., *Modern Ceramic Engineering*. Marcel Dekker, New York, 1992.
39. Cranmer, D. C. and Richerson, D. W., *Mechanical Testing Methodology for Ceramic Design and Reliability*. Marcel Dekker, New York, 1998.
40. Laugier, M. T., New formula for indentation toughness in ceramics. *J. Mater. Sci. Lett*., 1987, **1987**, 6 355-356.
41. Bruggeman, D. A. G., Berechnung verschiedener physikalischer Konstanten von heterogenen Substanzen. *Ann. Phys*., 1935, **24**, 636–664.
42. McLachlan, D. S., Blaszkiewicz, M. and Newnham, R. E., Electrical resistivity of composites. *J. Am. Ceram. Soc*., 1990, **73**, 2187–2203.
43. Bates, J. L. and Garnier, J. E., Electrical conductivity of $MgAl_2O_3$ and $Y_3Al_5O_{12}$. *J. Am. Ceram. Soc*., 1981, **64**, C138–141.